

1 **Title:**

2 **NADH biofluoro-shifting to red light toward multi-**  
3 **wavelength imaging application of VOCs**

4  
5

6 **Authors and affiliation**

7 Kenta Iitani<sup>a</sup>, Rintaro Miura<sup>b</sup>, Jifu Lim<sup>b</sup>, Ryotaro Ishida<sup>b</sup>, Kenta Ichikawa<sup>a</sup>, Koji Toma<sup>c</sup>, Kohji

8 Mitsubayashi<sup>a, b, \*</sup>

9

10 *<sup>a</sup> Department of Biomedical Devices and Instrumentation, Institute of Biomaterials and Bioengineering,*

11 *Tokyo Medical and Dental University, 2-3-10 Kanda-Surugadai, Chiyoda-ku, Tokyo 101-0062, Japan*

12 *<sup>b</sup> Graduate School of Medical and Dental Sciences, Tokyo Medical and Dental University, 1-5-45*

13 *Yushima, Bunkyo-ku, Tokyo 113-8510, Japan*

14 *<sup>c</sup> College of Engineering, Shibaura Institute of Technology, 3-7-5 Toyosu, Koto-ku, Tokyo 135-8548,*

15 *Japan*

16

17 **\*Corresponding author:**

18 *K. Mitsubayashi, Tel.: +81 3 5280 8091, Fax: +81 3 5280 8094, E-mail: m.bdi@tmd.ac.jp*

19

20

21 **Abstract**

22 In breath and transdermal gas, which contain thousands of volatile organic compounds  
23 (VOCs), selective simultaneous measurement of multiple VOCs is considered effective for  
24 noninvasive pharmacokinetic and metabolic tracking. Enzymatic optical biosensors with high  
25 selectivity and sensitivity have potential for simultaneous sensing and imaging of multiple  
26 VOCs by wavelength discrimination, but most enzymatic optical biosensors emit blue light  
27 region (400–500 nm). In this study, we investigated the possibility of red shifting the  
28 wavelength of luminol chemiluminescence (CL) and NADH fluorescence (FL), which emits  
29 blue light, for multiplexed VOCs imaging. Luminol CL and NADH FL were converted to red  
30 by addition of rhodamine B and by resorufin (excitation 560 nm, fluorescence 590 nm) which  
31 induced by diaphorase (DP) with resazurin. The results showed that resorufin was suitable for  
32 multiplexing because the spectrum overlap with blue region was minimal. In addition, a DP-  
33 immobilized cotton mesh enabled spatiotemporal imaging of NADH mist spray at optimal of  
34 various conditions (buffer pH = 6.5, DP amount = 60 U/cm<sup>2</sup>, initial resazurin = 100 μM) with  
35 fast response (90% response time = 10 s). Furthermore, the NADH detection sensitivity was  
36 sufficient for VOCs imaging with red light in combination with NADH-dependent enzymes. In  
37 the future, this technique can be used for simultaneous imaging of multiple VOCs in the same  
38 region of interest.

39

40 **Keywords:**

41 Image sensing, NADH, resorufin, diaphorase, biosensor, immobilization

42

## 43 **Introduction**

44       Assessment of metabolic function and disease diagnosis typically involves blood  
45 samples that require invasive collection. On the other hand, exhaled breath and transdermal  
46 gases can be collected noninvasively.<sup>1,2</sup> Therefore, they can be used for high-frequently medical  
47 check-up or health monitoring. Those exhaled breath and transdermal gases contain blood-  
48 borne volatile organic compounds (VOCs).<sup>3,4</sup> Since some of them are produced or removed by  
49 internal metabolism, they can be used to monitor biochemical status.<sup>5-7</sup> If VOCs in breath and  
50 transdermal gases can be easily measured and longitudinal VOCs changing profiles can be  
51 accumulated, it may be possible to detect metabolic abnormalities caused by diseases and  
52 infections from changes in VOCs concentrations. It was reported that nearly 1,500 different  
53 trace concentration of VOCs are contained in exhaled breath.<sup>8</sup> This means that highly selective  
54 and sensitive system is required for human-borne VOCs measurement. At the basic research  
55 level, analytical systems with high sensitivity and high selectivity, such as gas chromatography-  
56 mass spectrometry, are used.<sup>9,10</sup> However, it is impossible to utilize these analytical systems for  
57 healthy people on daily basis. Therefore, development various types of easy-to-use gas sensors  
58 that are small enough to be owned by individuals is under way.<sup>11-21</sup>

59       Currently, many gas sensors face the challenge of selectivity. To address this challenge,  
60 we are developing gas sensors that focus on the molecular recognition ability of enzymes.<sup>22,23</sup>  
61 The enzyme is suitable for human-borne VOC sensors that require selectivity because of its  
62 substrate specificity. Furthermore, the use of light for quantification of enzymatic reactions  
63 enables highly sensitive measurement.

64       One of the advantages of using light as a measurement medium is that distributions  
65 (spatial information) can be easily obtained.<sup>24,25</sup> If there is a mechanism for light intensity to  
66 vary with VOCs concentration in space, the spatiotemporal distribution of VOCs concentrations  
67 can be evaluated.<sup>26,27</sup> Another advantage is that specific wavelengths can be easily isolated to

68 measure based on multiband or hyperspectral imaging technique.<sup>28,29</sup> In principle, it is possible  
69 to respond to different VOCs at different wavelengths and simultaneously measure multiple  
70 VOCs in the same space, which allowed to monitoring the metabolic kinetics of  
71 pharmaceuticals and tracking multiple VOCs associated with diseases noninvasively. The  
72 utility of optical measurement for simultaneous measurement of multiple substances is well  
73 known in molecular biology. For instance, Chen *et al.* used excitation spectral microscopy to  
74 achieve simultaneous imaging of 10 different fluorophores with less than 0.5 % of cross-talk.<sup>30</sup>  
75 Using this method, one can simultaneously measure the distribution of 10 different molecules,  
76 proteins, organelles, and etc. labeled with different fluorophores.

77 On the other hand, label-free enzyme-based optical biosensors, which are easily  
78 deployed for continuous measurement, are limited in the wavelengths-bands they can use. For  
79 example, chemiluminescence (CL) produced by the luminol-horse radish peroxidase (HRP)  
80 system and autofluorescence (FL) of reduced nicotinamide adenine dinucleotide (NADH) are  
81 commonly used in label-free enzyme-based optical biosensors.<sup>31</sup> The wavelength of these lights  
82 almost overlap at 400–500 nm. While probes that can convert the wavelength of NADH FL  
83 have been developed,<sup>32–34</sup> their accessibility is limited because most of them must be  
84 synthesized on their own. This has been a challenge to realize multiplexed enzyme biosensors  
85 by using different wavelength of light in the same space.

86 A method for measuring NADH concentration by fluorescence at red region (500–600  
87 nm) has been used by using diaphorase (DP), which reduce resazurin with NADH as a substrate  
88 to resorufin with its fluorescence (ex 560 nm, fl 590 nm).<sup>35,36</sup> Another known method is to mix  
89 fluorophore in the luminol CL reaction solution and change the emission color by energy  
90 transfer.<sup>37,38</sup> However, with best of our knowledge, attempts at macroscopic chemical imaging  
91 using these simple light color changing methods are lacking. In this study, we compared luminol  
92 CL + fluorophore and NADH-DP-resazurin system for multiplexing with blue-colored light. In

93 addition, quantitative chemical imaging applicable to enzymatic optical biosensors was  
94 discussed using a method suitable for multi-wavelength imaging of VOCs.

95

## 96 **Experimental methods**

### 97 **Reagents**

98 HRP (product# 169-10791, >100 U/mg) was purchased from FUJIFILM Wako  
99 Chemicals, Japan. DP (product# 46446003, from *Clostridium Kluveri*, 181 U/mg powder) was  
100 purchased from Oriental Yeast, Japan. Glutaraldehyde (GA, 25%, product# 079-00533) was  
101 from FUJIFILM Wako Chemicals. Hydrogen peroxide (30.0–35.5%, product# 18084-00) was  
102 from Kanto Kagaku, Japan. Luminol (product# 127-02581) and RB (product# 183-00122) were  
103 from FUJIFILM Wako Chemicals. NADH (product# 44327000) was from Oriental Yeast.  
104 Resazurin sodium salt (product# 191-07581) and resorufin (product# 73144) were from  
105 FUJIFILM Wako Chemicals and Sigma-Aldrich, USA. Acetate buffer (AB) was prepared by  
106 acetic acid (product# 017-00256, FUJIFILM Wako Chemicals) and sodium acetate (product#  
107 192-01075, FUJIFILM Wako Chemicals). Phosphate buffer (PB) was made with potassium  
108 dihydrogen phosphate (product# 169-04245; FUJIFILM Wako Chemicals) and disodium  
109 hydrogen phosphate (product# 197-02865; FUJIFILM Wako Chemicals). Tris-HCl buffer (TB)  
110 was prepared by hydrochloric acid (product# 083-3485; FUJIFILM Wako Chemicals) and  
111 2-amino-2-hydroxymethyl-1,3-propanediol (product# 013-16385; FUJIFILM Wako Chemicals).  
112 Trisodium phosphate buffer (TPB) was prepared by potassium dihydrogen phosphate and  
113 trisodium phosphate dodecahydrate (product# 191-082885, FUJIFILM Wako Chemicals). All  
114 buffers made using ultrapure water prepared by PURELAB Flex (ELGA LabWater, U.K.).

115

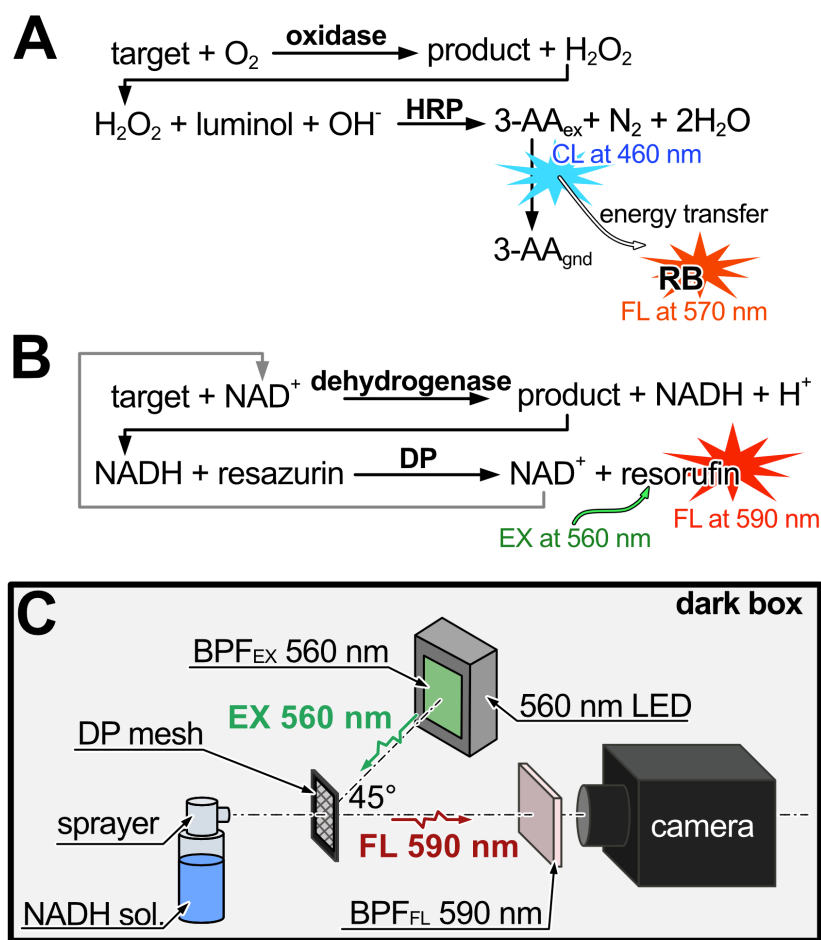
### 116 **Comparison of detection method for target chemicals using red light**

117 Figure 1A shows the measuring principle by target molecule by red light based on

118 luminol CL. Many oxidases consume oxygen to produce hydrogen peroxide when oxidizing  
119 the target molecule in the reaction. This hydrogen peroxide triggers luminol CL in the presence  
120 of luminol and HRP. Under normal conditions, luminol emission is blue with a central  
121 wavelength around 450–460 nm, but when RB is added to the reaction, energy transfer occurs,  
122 and RB FL (maximum wavelength around 590 nm) is emitted. Various other fluorophores can  
123 be used besides RB, but RB was selected based on its difference in peak wavelength from 400–  
124 500 nm. Fig. 1B shows a scheme for generating resorufin by triggering NADH produced by the  
125 reaction of NADH-dependent enzymes. It is possible to quantify the change in target molecule  
126 concentration using red light by resorufin FL (excitation 560 nm, emission 590 nm).

127         In the experiments, the optical wavelength spectra produced by each reaction were  
128 examined. In the case of luminol + RB, 1 mg of HRP and 1 mg of RB were dissolved in a  
129 luminol solution prepared at 5 mM using TB (at pH 10.1, 0.1 M). Hydrogen peroxide prepared  
130 to 10 mM was added to a cuvette containing this mixture and scanned for emission wavelength  
131 using a fluorescence spectrophotometer (product# F-7000, Hitachi High-Tech, Japan). Note  
132 that the cuvettes were shielded with a black cloth to avoid exposure to any excitation light. In  
133 the evaluation of an NADH-DP-resazurin system, resazurin was dissolved in PB (at pH 8.0,  
134 0.1M) to prepare a 10  $\mu$ M resazurin solution, and 1 mg of DP was added to prepare a resazurin-  
135 DP solution. Further 100  $\mu$ M NADH solution was added, and FL spectra were obtained at an  
136 excitation wavelength of 560 nm.

137



138

139 **Figure 1.** The target molecule detection method based on (A) luminol chemiluminescence and  
 140 (B) NADH-mediated cascade reaction. The red light was used to detect molecule in both  
 141 methods. (C) The setup for imaging of NADH in mist spray.

142

### 143 **Evaluation of dynamic ranges of NADH and resorufin using fluorescence macro imaging**

144 The same camera (product# C15550-20UP, Hamamatsu Photonics, Japan) was then  
 145 used to acquire FL intensities emitted from various concentrations of NADH and resorufin to  
 146 obtain the quantitative characteristics of each molecule. In the experiment, the optical system  
 147 shown in Figs. S1A or S1B was used to observe NADH or resorufin, respectively. The NADH  
 148 imaging system consisted of a ring-type UV-LED (custom-made, emission 340 nm, DOWA  
 149 electronics, Japan) equipped with a bandpass filter (BPF, product#65-209,  $492 \pm 5$  nm, Edmond  
 150 optics, USA) for FL and a BPF (custom-made,  $340 \pm 42.5$  nm, HOYA candeo optronics, Japan)

151 for excitation, as used in previous studies. An imaging target was placed at a distance of 60 mm  
152 from the lens. The resorufin imaging system consisted of a light source with five Yellow Green  
153 LEDs (product# 4903670676543, 550-570 nm, LED Generic, Japan), a BPF for excitation  
154 (product# HMZ0560,  $560 \pm 5$  nm, Asahi Spectra, Japan), an imaging target, a BPF for FL  
155 (product# HMX0590,  $590 \pm 5$  nm, Asahi Spectra, Japan), and a camera. All components were  
156 arranged on the same optical axis. In both imaging experiments, FL emitted from cotton mesh  
157 (product# 002-20377,  $1.5 \times 1.5$  cm, Iwatsuki, Japan) soaked with 80  $\mu$ L of NADH or resorufin  
158 solution prepared in PB (at pH 7.0, 0.1 M) was captured by the camera. The concentration of  
159 NADH or resorufin soaked in the cotton mesh was varied from 1 nM to 100 mM or 1 nM to  
160 100  $\mu$ M, respectively. Cotton mesh soaked with PB was also captured to obtain background  
161 images. The camera exposure time was set to 1 s for all experiments. The FL images were  
162 analyzed by using ImageJ2.<sup>39</sup> The entire area of the cotton mesh was set as the region of interest  
163 and the average intensity was calculated. Calibration curves were obtained by plotting the  
164 difference of average intensity between each concentration and background and curve fitting  
165 using Origin 2015.

166

### 167 **Optimization of reaction conditions of DP**

168 In the case of imaging of NADH by red light, DP was immobilized on cotton mesh, and  
169 DP-immobilized mesh was used in the experiment. For DP immobilization, first, 100  $\mu$ M of PB  
170 (at pH 6.5, 0.1 M) containing 60 U/cm<sup>2</sup> DP was dropped onto a  $1.5 \times 1.5$  cm cotton mesh and  
171 placed in a refrigerator for 1 h. Next, 18  $\mu$ L of 2.5 v/v% GA (in PB at pH 7.0, 0.1 M) was added  
172 dropwise and placed in the refrigerator for 1.5 h. Finally, the DP-immobilized cotton mesh was  
173 rinsed with 300  $\mu$ L of PB (at pH 6.5, 0.1 M). The prepared DP-immobilized mesh was placed  
174 in the optical system with 80  $\mu$ L drops of 100  $\mu$ M resazurin solution prepared in PB at pH 7.5  
175 (see Fig. 1C). Excitation light was irradiated and 100  $\mu$ M NADH solution was sprayed from



176 the back of the DP-immobilized mesh white camera took video. In displaying the distribution  
177 of FL intensity, the difference image between the images taken at the start of recording and  
178 those taken after that was calculated.

179 We then searched for optimal values for the buffer pH of the resazurin solution, the  
180 amount of DP used for immobilization, and the initial concentration of resazurin solution, which  
181 are expected to have a significant impact on the NADH quantification performance. For the  
182 selection of buffer pH, 100  $\mu\text{M}$  of resazurin solutions were prepared using AB (at pH 4.0–6.0),  
183 PB (at pH 5.5–7.5), TB (at pH 7.5–9.0), and TPB (at pH 8.0–9.0). The prepared resazurin  
184 solution was soaked into a DP-immobilized mesh with 60  $\text{U}/\text{cm}^2$  DP. The output response was  
185 observed by spraying 50  $\mu\text{M}$  NADH solution. Subsequently, DP-immobilized meshes with DP  
186 amounts of 0.6, 3, 6, 30, 60, and 100  $\text{U}/\text{cm}^2$  were soaked with 100  $\mu\text{M}$  resazurin solution  
187 prepared in PB (at pH 6.5, 0.1 M) and sprayed with 50  $\mu\text{M}$  NADH to determine DP amount for  
188 immobilization. Furthermore, the optimal initial resazurin concentration was examined by  
189 soaking the 60  $\text{U}/\text{cm}^2$  DP-immobilized mesh with 10, 30, 50, 100, 200, 300, and 1000  $\mu\text{M}$   
190 resazurin solution prepared in PB (at pH 6.5, 0.1 M) and spraying 50  $\mu\text{M}$  NADH solution.

191

## 192 **Image analysis of dynamic changes of DP-mediated fluorescence**

193 Since the resorufin produced by the DP reaction remains after the reaction stops, it is  
194 impossible to know at what time to reaction occurred without observing all images. Therefore,  
195 we examined time-domain image differential analysis to calculate the DP reaction rate to  
196 observe the change in output in response to NADH spraying. In this section, FL images obtained  
197 by spraying 100  $\mu\text{M}$  NADH onto 60  $\text{U}/\text{cm}^2$  DP-immobilized mesh soaked with 80  $\mu\text{L}$  of 100  
198  $\mu\text{M}$  resazurin were analyzed in accordance with previous studies. First, background subtraction  
199 images were calculated. Then differential images were calculated using Equation (1).

$$\text{differential image} = \frac{\text{FL image}_i - \text{FL image}_{(fps \times \Delta t)}}{\Delta t} \quad (1)$$

200 Where  $\Delta t = 10$ ,  $fps = 1$ ,  $i > 10$

201

## 202 **Quantitative characteristics for DP-mediated NADH image sensing**

203 NADH solutions from 1 nM to 100  $\mu\text{M}$  were sprayed onto the DP-immobilized mesh  
204 using optimized conditions for imaging of NADH by resorufin FL. The resulting FL images  
205 and calculated differential images were used to evaluate the quantitative characteristic of  
206 NADH.

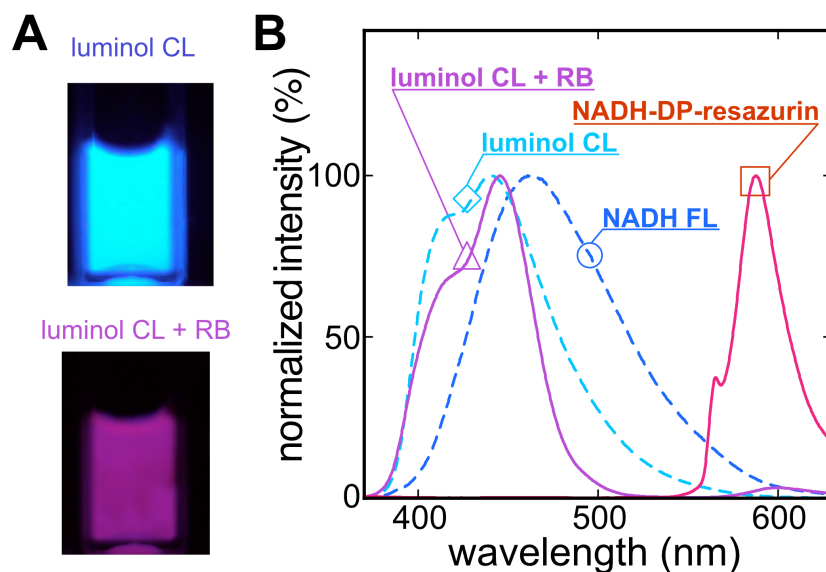
207

## 208 **Results and Discussions**

### 209 **Spectral comparison for wavelength-based chemical imaging**

210 Figure 2A shows camera images of luminol CL and luminol CL + RB generated in  
211 cuvettes. These images show that luminol CL + RB has a visually different emission color than  
212 blue. The emission spectra of NADH FL, NADH-DP-resazurin (resorufin FL), luminol CL, and  
213 luminol CL + RB were normalized by the peak value of each spectrum and compared (see Fig.  
214 2B). The results show that luminol CL and luminol CL + RB have a smaller difference in  
215 spectral shape compared to visual differences. The addition of RB reduced the light intensity  
216 around 420 nm and slightly sharpened the spectrum shape from 400–500 nm. In addition, a  
217 small and broad rise was observed around 600 nm. This spectral shape was considered to have  
218 a large overlap with NADH FL and luminol CL, which show blue light, making wavelength  
219 separation difficult during multiplexing measurements. In contrast, resorufin FL emitted via  
220 NADH-DP-resazurin system has a relatively sharp spectrum centered at 590 nm, with minimal  
221 overlap in the spectrum with the blue light at 400–500 nm. The shoulder around 560 nm was  
222 considered caused by the excitation light reaching the detector. As a result, the method using  
223 resorufin FL could be easily combined with luminol CL or NADH FL. In conclusion, we

224 focused on the NADH-DP-resazurin system to investigate the possibility of chemical imaging  
225 with red light.



226  
227 **Figure 2.** (A) photo images of luminol CL and luminol CL with RB, and (B) spectrum of (◇)  
228 luminol CL, (Δ) luminol CL + RB, (○) NADH FL, and (□) DP-induced resorufin FL. All  
229 spectra were normalized by peak maximum intensity.

230

### 231 Sensitivity of the system on NADH FL and resorufin FL

232 Figures 3A and 3B show the results of microimaging of NADH FL and resorufin FL.  
233 The relationship between the average FL intensity of the acquired images and the concentrations  
234 of NADH and resorufin can be fitted by Equations (2) and (3) in the concentration ranges of  
235 0.1–10000  $\mu\text{M}$  and 0.03–300  $\mu\text{M}$ , respectively. The limit of quantification (LoQ) calculated  
236 from the 10-fold value of the background standard deviation was 276 nM and 43 nM for NADH  
237 and resorufin, respectively. The NADH-DP-resorufin system requires an enzymatic reaction for  
238 the determination of NADH concentration. In general, the additional steps in a cascade reaction,  
239 lower the efficiency of the final product formation. Thus, the NADH-DP-resorufin system was  
240 expected to have lower detection sensitivity for NADH than the method using NADH FL  
241 directly for quantification. However, the sensitivity to resorufin was higher than that to NADH,

242 suggesting that the effect of the enzymatic reaction on sensitivity may be counterbalancing.  
 243 This difference in detection sensitivity at low concentrations can be explained by FL quantum  
 244 yield which is defined as the ratio of the number of photons emitted as FL to the number of  
 245 photons absorbed. If the FL quantum yield is low, the FL intensity obtained will be low even if  
 246 the same level of photoexcitation is possible. The absolute FL quantum yield of NADH in water  
 247 is calculated to be 2.1%,<sup>40</sup> while the FL quantum yield of resorufin was around 74%.<sup>41</sup>

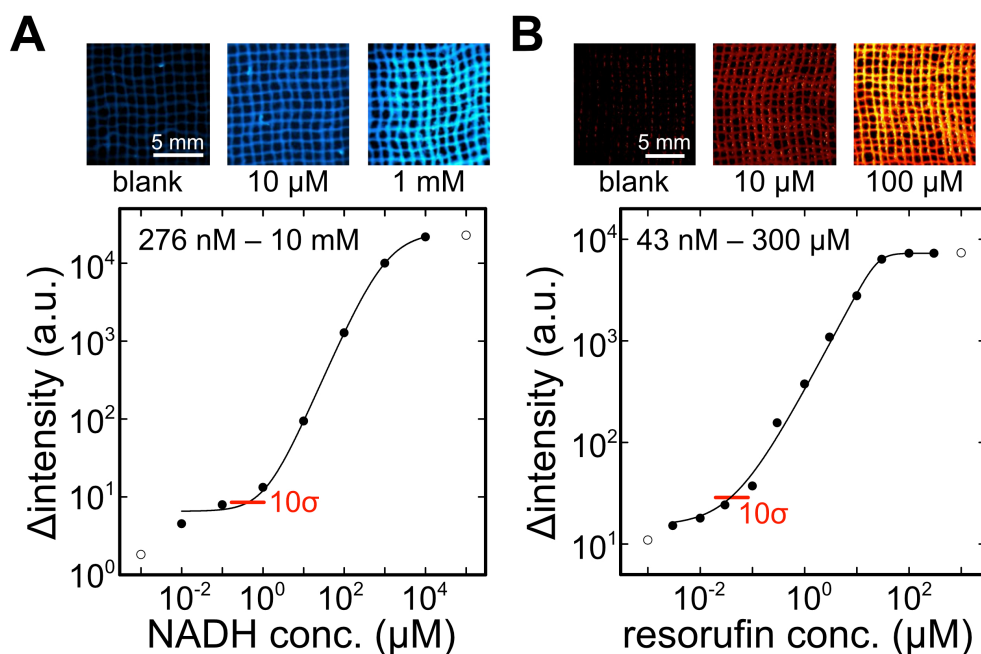
$$\Delta \text{intensity (a.u.)} = A + \frac{B - A}{\left\{1 + \frac{[\text{NADH conc. } (\mu\text{M})]^{-D}}{C}\right\}^E} \quad (2)$$

248 Where A = 6.540, B=2.502×10<sup>4</sup>, C=1062, D = 0.9488, and E = 1.2743

$$\Delta \text{intensity (a.u.)} = A + \frac{B - A}{\left\{1 + \frac{[\text{resorufin conc. } (\mu\text{M})]^{-D}}{C}\right\}^E} \quad (3)$$

249 Where A = 15.19, B=7291, C=25.38, D = 3.201, and E = 0.3022

250



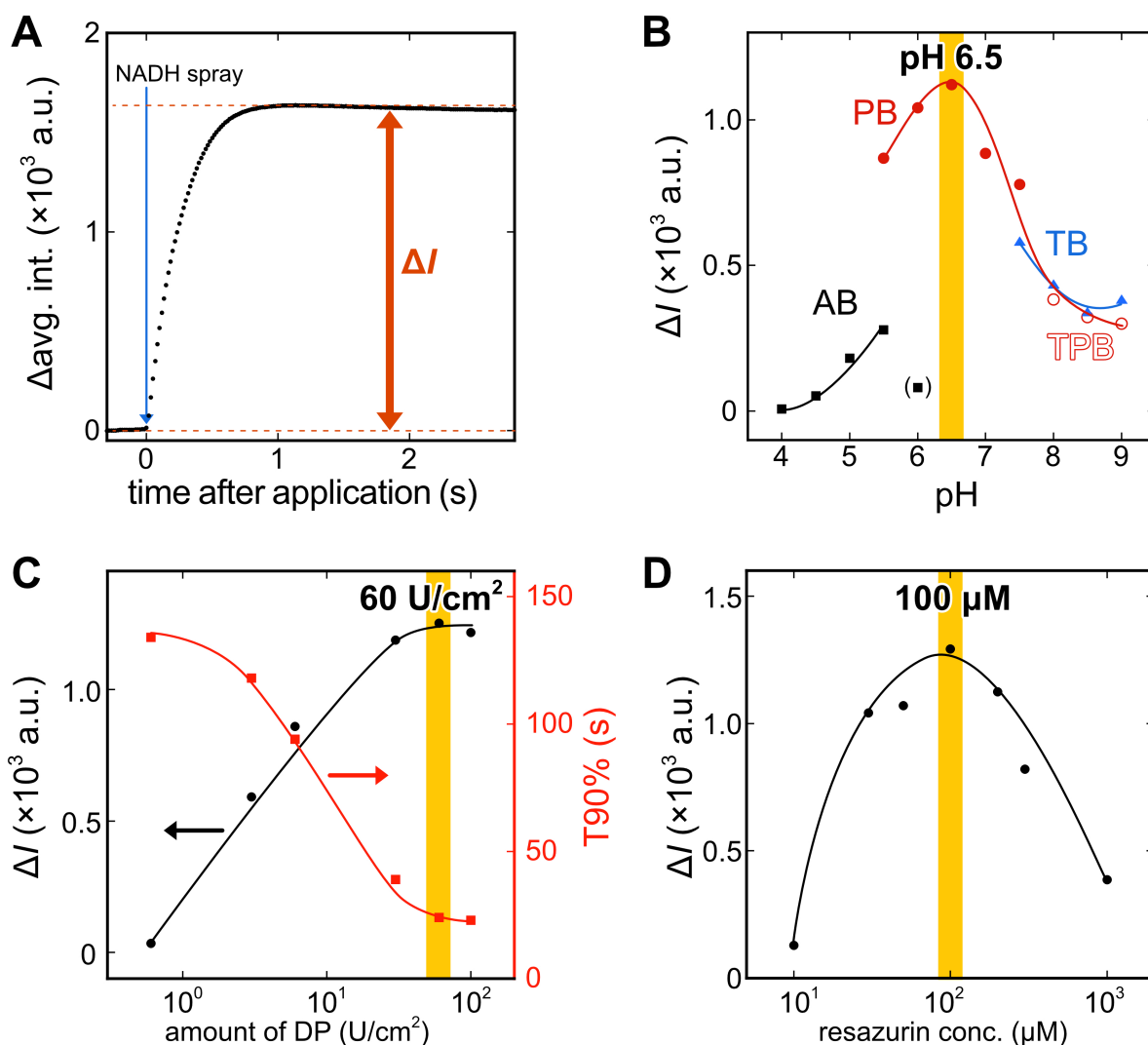
251

252 **Figure 3.** Results of image sensing of (A) NADH and (B) resorufin based on fluorescence

253

254 **Optimum conditions of buffer pH, immobilized amount, and initial resazurin**  
 255 **concentration for NADH-DP-resazurin system**

256 Figure 4A shows the change over time in the FL intensity of resorufin produced when a  
257 resazurin-soaked DP-immobilized mesh was sprayed with NADH mist spray. The FL intensity  
258 of resorufin increased immediately after spraying, and it could be observed that the FL reached  
259 its equilibrium value. The difference between the baseline and equilibrium values was defined  
260 as  $\Delta I$ , and the 90% response time ( $T_{90\%}$ ) was calculated to be 31 s. Optimization of the NADH-  
261 DP-resazurin system was performed using  $\Delta I$  as an indicator. The maximum value of  $\Delta I$  was  
262 obtained at pH 6.5 among various buffer pH (response curve shown in Fig. S2A). The  
263 relationship between the amount of DP used for immobilization,  $\Delta I$ , and  $T_{90\%}$  showed that the  
264 use of 60 U/cm<sup>2</sup> DP was the best (see Fig. 4C, response curve shown in Fig. S2B). In addition,  
265 the effect of the initial resazurin concentration on  $\Delta I$  was evaluated. As shown in Fig. 4D, a  
266 maximum value was observed at 100  $\mu$ M, and higher additions resulted in a decrease in  $\Delta I$   
267 (response curve shown in Fig. S2C). Resazurin has high absorbance at 560 nm and 590 nm as  
268 shown in Figs. S3. Therefore, if a large amount of abundant resazurin remains after the reaction,  
269 excitation of resorufin is blocked by resazurin, and the resulting resorufin FL is also absorbed  
270 by resazurin. Based on the above experimental results, the reaction conditions for the NADH-  
271 DP-resazurin system were set to pH 6.5, DP amount 60 U/cm<sup>2</sup>, and resazurin concentration 100  
272  $\mu$ M.



273

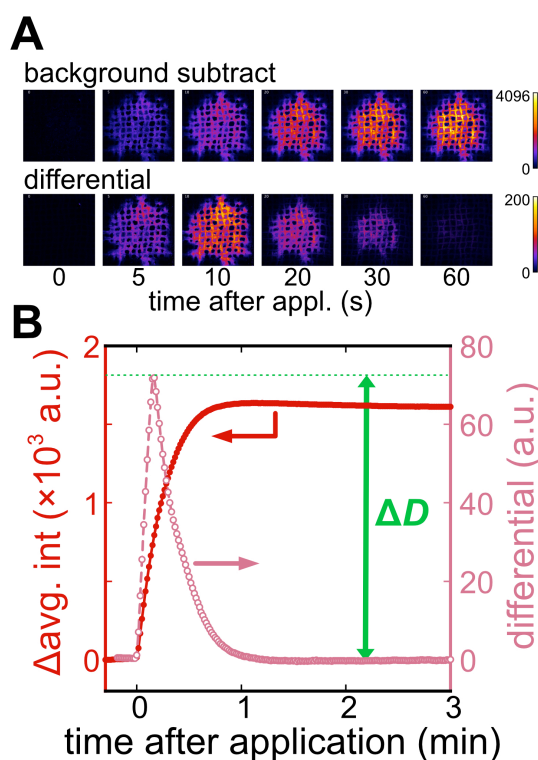
274 **Figure 4.** (A) Time course of the fluorescence change by applying NADH spray. (B) pH  
 275 dependency of fluorescence change caused by applying NADH spray. (C) Relationship between  
 276 the amount of DP used for immobilization. (D) Effect of initial resazurin concentration on  $\Delta I$ .

277

## 278 Spatiotemporal imaging of NADH via DP-mediated resorufin FL

279 Figure 5A shows FL images of resorufin on a DP-immobilized mesh produced by  
 280 spraying NADH solution and a differential image (videos are shown in Supplemental Videos 1  
 281 and 2). By using differential analysis, it is easy to determine whether or not NADH currently  
 282 being applied from the single frame as shown in these images. The numerical values of these

283 images showed that the T90% of peak  $\Delta D$  is shorter than that of the FL intensity analysis (from  
284 31 s to 10s).



285  
286 **Figure 5.** (A) Images of background subtract FL and differential analysis (B) Time course of  
287 fluorescence changes and differential value.

288

### 289 Quantitative characteristics of NADH by using DP-mediated resorufin FL

290 Figures 6A and 6B show the changes over time of resorufin FL intensity and the  
291 differential value obtained by spraying different concentrations of NADH on DP-immobilized  
292 meshes under optimal conditions. The FL intensity exhibited equilibrium values that carried  
293 with the concentration of NADH, and  $\Delta D$  changed accordingly. NADH calibration curves were  
294 calculated from the obtained  $\Delta I$  and  $\Delta D$ , which could be fitted by Equations (4) and (5) in the  
295 concentration range of 0.01–100  $\mu\text{M}$ , respectively. The LoQs were 0.7 and 2.7  $\mu\text{M}$  for  $\Delta I$  and  
296  $\Delta D$ , respectively. These LoQs were 2.5- and 9.6-fold higher than those obtained when NADH  
297 itself was excited (0.28  $\mu\text{M}$ ) taken by the same camera, indicating that the sensitivity was  
298 reduced by the enzymatic reaction, which was mentioned earlier. On the other hand, the LoQ

299 of NADH in the previous systems we have reported was tens of  $\mu\text{M}$  (using a UV-LED sheet  
 300 array and a HEED-HARP camera) and hundreds of nM (using a ring-type UV-LED and a  
 301 CMOS RGB camera). This suggests that the optical system and NADH-DP-resazurin system  
 302 developed in this study can be applied to VOC imaging by red light in combination with other  
 303 NADH-dependent enzymes.

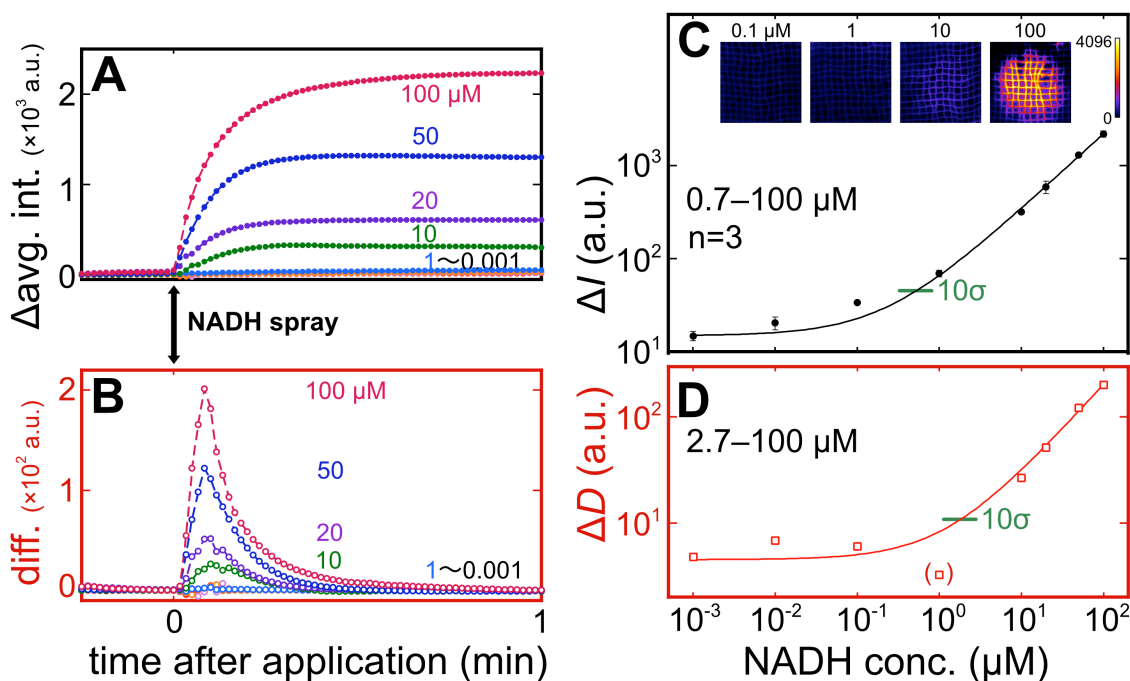
$$\Delta I(\text{a.u.}) = A + B \times [\text{NADH conc. } (\mu\text{M})]^C \quad (3)$$

304 Where  $A = 14.798$ ,  $B=51.061$ ,  $C=0.81505$

$$\Delta D(\text{a.u.}) = A + B \times [\text{NADH conc. } (\mu\text{M})]^C \quad (3)$$

305 Where  $A = 4.5013$ ,  $B=3.7908$ ,  $C=0.86115$

306



307  
 308 **Figure 6.** Response curves of (A) FL change and (B) its differential with different concentration  
 309 of NADH. Calibration curve for the NADH concentration based on (C)  $\Delta I$  and (D)  $\Delta D$ .

310

### 311 Conclusion

312 In this study, we investigated the methodology of chemical imaging with red light to  
 313 achieve multiplexing with blue light, which is frequently used in enzymatic optical biosensors.



314 The suitability of luminol CL + RB and NADH-DP-resazurin system as candidates for the use  
315 of red light for quantitative imaging of hydrogen peroxide or NADH was evaluated. The results  
316 showed that resorufin, an FL molecule produced by the NADH-DP-resazurin system, has a  
317 minimal wavelength overlap with luminol CL and NADH FL. Therefore, we optimized the  
318 reaction conditions of the NADH-DP-resazurin system and found that the detection sensitivity  
319 of NADH was maximized by using a 100  $\mu\text{M}$  resazurin solution prepared with PB at pH 6.5 for  
320 60  $\text{U}/\text{cm}^2$  DP-immobilized on a cotton mesh. Spatiotemporal imaging of resorufin produced by  
321 the NADH-DP-resazurin system was also achieved by time-domain image differential and a  
322 good response was observed ( $T_{90\%} = 10 \text{ s}$ ). The LoQ of NADH by using the NADH-DP-  
323 resazurin system was 0.7 and 2.7  $\mu\text{M}$  based on FL intensity and reaction rate, respectively.  
324 Those LoQs were comparable to the LoQ of NADH of our previous system for VOC imaging  
325 using NADH-dependent enzymes. In the future, this system will be combined with NADH-  
326 dependent enzymes for red fluorescence VOC imaging and multiplexed with a blue  
327 fluorescence VOC imaging method to be applied for same-space imaging of multiple VOCs at  
328 the same time.

329 **Supporting information**

330 The supporting Information is available free of charge at XXX.

331 Additional figures: **Figure S1.** Response curves of the base system against standard acetone  
332 gas; **Figure S2.** Typical response curves in evaluations of (A) buffer pH, (b) amount of DP for  
333 immobilization, (C) concentration of initial resazurin; **Figure S3.** Absorption spectrum of  
334 resazurin at different concentrations. (PDF)

335

336 **Supplemental Video 1.** 30-times fast forward moving images of FL generated on DP-  
337 immobilized mesh by applying NADH mist spray.

338 **Supplemental Video 2.** 30-times fast forward moving images of results of time-domain image  
339 differential analysis on FL images of Supplemental Video 1.

340

341 **Notes**

342 The authors declare that they have no known competing financial interests or personal  
343 relationships that could have appeared to influence the work reported in this paper.

344

345 **Acknowledgments**

346 This work was supported by the Japan Society for the Promotion of Science (JSPS)  
347 KAKENHI Grant Numbers JP21H04888, JP22K18416, and JP23H03864, JST ACT-X Grant  
348 Number JPMJAX23K2, the Cooperative Research Project of Research Center for Biomedical  
349 Engineering.

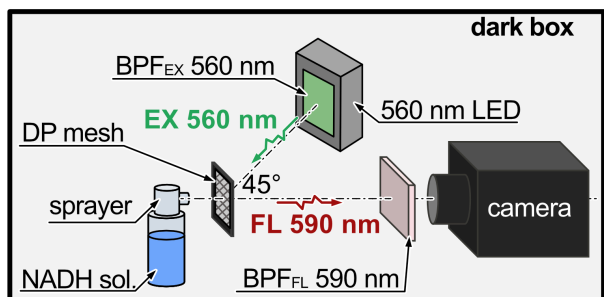
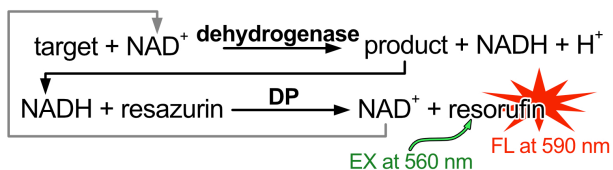
350

- 352 (1) Lawal, O.; Ahmed, W. M.; Nijsen, T. M. E.; Goodacre, R.; Fowler, S. J. Exhaled Breath  
353 Analysis: A Review of ‘Breath-Taking’ Methods for off-Line Analysis. *Metabolomics*  
354 **2017**, *13* (10), 110. <https://doi.org/10.1007/s11306-017-1241-8>.
- 355 (2) S., K.; Saquib, M.; Poojary, H.; Illanad, G.; Valavan, D.; M, S.; Nayak, R.; Mazumder,  
356 N.; Ghosh, C. Skin Emitted Volatiles Analysis for Noninvasive Diagnosis: The Current  
357 Advances in Sample Preparation Techniques for Biomedical Application. *RSC Adv.* **2024**,  
358 *14* (17), 12009–12020. <https://doi.org/10.1039/D4RA01579G>.
- 359 (3) Shirasu, M.; Touhara, K. The Scent of Disease: Volatile Organic Compounds of the  
360 Human Body Related to Disease and Disorder. *J. Biochem. (Tokyo)* **2011**, *150* (3), 257–  
361 266. <https://doi.org/10.1093/jb/mvr090>.
- 362 (4) *Volatile Biomarkers: Non-Invasive Diagnosis in Physiology and Medicine*, 1st ed.;  
363 Amann, A., Smith, D., Eds.; Elsevier: Amsterdam ; Boston, 2013.
- 364 (5) Davies, S. J.; Španěl, P.; Smith, D. Breath Analysis of Ammonia, Volatile Organic  
365 Compounds and Deuterated Water Vapor in Chronic Kidney Disease and during Dialysis.  
366 *Bioanalysis* **2014**, *6* (6), 843–857. <https://doi.org/10.4155/bio.14.26>.
- 367 (6) Güntner, A. T.; Weber, I. C.; Schon, S.; Pratsinis, S. E.; Gerber, P. A. Monitoring Rapid  
368 Metabolic Changes in Health and Type-1 Diabetes with Breath Acetone Sensors. *Sens.*  
369 *Actuators B Chem.* **2022**, *367*, 132182. <https://doi.org/10.1016/j.snb.2022.132182>.
- 370 (7) Chen, X.; Zhang, K.; Yin, Z.; Fang, M.; Pu, W.; Liu, Z.; Li, L.; Sinues, P.; Dallmann, R.;  
371 Zhou, Z.; Li, X. Online Real-Time Monitoring of Exhaled Breath Particles Reveals  
372 Unnoticed Transport of Nonvolatile Drugs from Blood to Breath. *Anal. Chem.* **2021**, *93*  
373 (12), 5005–5008. <https://doi.org/10.1021/acs.analchem.1c00509>.
- 374 (8) Drabińska, N.; Flynn, C.; Ratcliffe, N.; Belluomo, I.; Myridakis, A.; Gould, O.; Fois, M.;  
375 Smart, A.; Devine, T.; Costello, B. D. L. A Literature Survey of All Volatiles from  
376 Healthy Human Breath and Bodily Fluids: The Human Volatilome. *J. Breath Res.* **2021**,  
377 *15* (3), 034001. <https://doi.org/10.1088/1752-7163/abf1d0>.
- 378 (9) Majchrzak, T.; Wojnowski, W.; Lubinska-Szczygeł, M.; Różańska, A.; Namieśnik, J.;  
379 Dymerski, T. PTR-MS and GC-MS as Complementary Techniques for Analysis of  
380 Volatiles: A Tutorial Review. *Anal. Chim. Acta* **2018**, *1035*, 1–13.  
381 <https://doi.org/10.1016/j.aca.2018.06.056>.
- 382 (10) Smith, D.; Španěl, P.; Demarais, N.; Langford, V. S.; McEwan, M. J. Recent  
383 Developments and Applications of Selected Ion Flow Tube Mass Spectrometry (SIFT-  
384 MS). *Mass Spectrom. Rev.* **2023**, e21835. <https://doi.org/10.1002/mas.21835>.
- 385 (11) Zhao, Y.; Liu, Y.; Han, B.; Wang, M.; Wang, Q.; Zhang, Y. Fiber Optic Volatile Organic  
386 Compound Gas Sensors: A Review. *Coord. Chem. Rev.* **2023**, *493*, 215297.  
387 <https://doi.org/10.1016/j.ccr.2023.215297>.
- 388 (12) Wang, L. Metal-Organic Frameworks for QCM-Based Gas Sensors: A Review. *Sens.*  
389 *Actuators Phys.* **2020**, *307*, 111984. <https://doi.org/10.1016/j.sna.2020.111984>.
- 390 (13) Shinde, P. V.; Rout, C. S. Magnetic Gas Sensing: Working Principles and Recent  
391 Developments. *Nanoscale Adv.* **2021**, *3* (6), 1551–1568.  
392 <https://doi.org/10.1039/D0NA00826E>.
- 393 (14) Minami, K.; Imamura, G.; Tamura, R.; Shiba, K.; Yoshikawa, G. Recent Advances in  
394 Nanomechanical Membrane-Type Surface Stress Sensors towards Artificial Olfaction.  
395 *Biosensors* **2022**, *12* (9), 762. <https://doi.org/10.3390/bios12090762>.
- 396 (15) Jha, R. K. Non-Dispersive Infrared Gas Sensing Technology: A Review. *IEEE Sens. J.*  
397 **2022**, *22* (1), 6–15. <https://doi.org/10.1109/JSEN.2021.3130034>.
- 398 (16) Gardner, E. L. W.; Gardner, J. W.; Udreă, F. Micromachined Thermal Gas Sensors—A  
399 Review. *Sensors* **2023**, *23* (2), 681. <https://doi.org/10.3390/s23020681>.

- 400 (17) Gaggiotti, S.; Della Pelle, F.; Mascini, M.; Cichelli, A.; Compagnone, D. Peptides, DNA  
401 and MIPs in Gas Sensing. From the Realization of the Sensors to Sample Analysis.  
402 *Sensors* **2020**, *20* (16), 4433. <https://doi.org/10.3390/s20164433>.
- 403 (18) Dey, A. Semiconductor Metal Oxide Gas Sensors: A Review. *Mater. Sci. Eng. B* **2018**,  
404 *229*, 206–217. <https://doi.org/10.1016/j.mseb.2017.12.036>.
- 405 (19) Chowdhury, N. K.; Bhowmik, B. Micro/Nanostructured Gas Sensors: The Physics behind  
406 the Nanostructure Growth, Sensing and Selectivity Mechanisms. *Nanoscale Adv.* **2021**, *3*  
407 (1), 73–93. <https://doi.org/10.1039/D0NA00552E>.
- 408 (20) Benhaddouch, T. E.; Pinzon, S. K.; Landi, D. M. C.; Marcial, J.; Mehta, P.; Romero, K.;  
409 Rockward, T.; Bhansali, S.; Dong, D. Review—Micro-Fuel Cell Principal Biosensors for  
410 Monitoring Transdermal Volatile Organic Compounds in Humans. *ECS Sens. Plus* **2022**,  
411 *1* (4), 041602. <https://doi.org/10.1149/2754-2726/aca95b>.
- 412 (21) Amiri, V.; Roshan, H.; Mirzaei, A.; Neri, G.; Ayesh, A. I. Nanostructured Metal Oxide-  
413 Based Acetone Gas Sensors: A Review. *Sensors* **2020**, *20* (11), 3096.  
414 <https://doi.org/10.3390/s20113096>.
- 415 (22) Arakawa, T.; Iitani, K.; Toma, K.; Mitsubayashi, K. Biosensors: Gas Sensors. In  
416 *Encyclopedia of Sensors and Biosensors (First Edition)*; Narayan, R., Ed.; Elsevier:  
417 Oxford, 2023; pp 478–504. <https://doi.org/10.1016/B978-0-12-822548-6.00066-2>.
- 418 (23) Mitsubayashi, K.; Toma, K.; Iitani, K.; Arakawa, T. Gas-Phase Biosensors: A Review.  
419 *Sens. Actuators B Chem.* **2022**, *367*, 132053. <https://doi.org/10.1016/j.snb.2022.132053>.
- 420 (24) Schäferling, M. The Art of Fluorescence Imaging with Chemical Sensors. *Angew. Chem.*  
421 *Int. Ed.* **2012**, *51* (15), 3532–3554. <https://doi.org/10.1002/anie.201105459>.
- 422 (25) Weckhuysen, B. M. Chemical Imaging of Spatial Heterogeneities in Catalytic Solids at  
423 Different Length and Time Scales. *Angew. Chem. Int. Ed.* **2009**, *48* (27), 4910–4943.  
424 <https://doi.org/10.1002/anie.200900339>.
- 425 (26) Iitani, K.; Toma, K.; Arakawa, T.; Mitsubayashi, K. Transcutaneous Blood VOC Imaging  
426 System (Skin-Gas Cam) with Real-Time Bio-Fluorometric Device on Rounded Skin  
427 Surface. *ACS Sens.* **2020**, *5* (2), 338–345. <https://doi.org/10.1021/acssensors.9b01658>.
- 428 (27) Iitani, K.; Ichikawa, K.; Toma, K.; Arakawa, T.; Mitsubayashi, K. Biofluorometric Gas-  
429 Imaging System for Evaluating the Ripening Stages of “La France” Pear Based on  
430 Ethanol Vapor Emitted via the Epicarp. *ACS Sens.* **2024**.
- 431 (28) Wang, Y. W.; Reder, N. P.; Kang, S.; Glaser, A. K.; Liu, J. T. C. Multiplexed Optical  
432 Imaging of Tumor-Directed Nanoparticles: A Review of Imaging Systems and  
433 Approaches. *Nanotheranostics* **2017**, *1* (4), 369–388. <https://doi.org/10.7150/ntno.21136>.
- 434 (29) Lee, H.; Kim, J.; Kim, H.-H.; Kim, C.-S.; Kim, J. Review on Optical Imaging Techniques  
435 for Multispectral Analysis of Nanomaterials. *Nanotheranostics* **2022**, *6* (1), 50–61.  
436 <https://doi.org/10.7150/ntno.63222>.
- 437 (30) Chen, K.; Li, W.; Xu, K. Super-Multiplexing Excitation Spectral Microscopy with  
438 Multiple Fluorescence Bands. *Biomed. Opt. Express* **2022**, *13* (11), 6048.  
439 <https://doi.org/10.1364/BOE.473241>.
- 440 (31) Blum, L. J.; Marquette, C. A. CHEMILUMINESCENCE-BASED SENSORS. In *Optical*  
441 *Chemical Sensors*; Baldini, F., Chester, A. N., Homola, J., Martellucci, S., Eds.; Springer  
442 Netherlands: Dordrecht, 2006; pp 157–178. [https://doi.org/10.1007/1-4020-4611-1\\_8](https://doi.org/10.1007/1-4020-4611-1_8).
- 443 (32) Zhou, Y.; Xu, Z.; Yoon, J. Fluorescent and Colorimetric Chemosensors for Detection of  
444 Nucleotides, FAD and NADH: Highlighted Research during 2004–2010. *Chem. Soc. Rev.*  
445 **2011**, *40* (5), 2222. <https://doi.org/10.1039/c0cs00169d>.
- 446 (33) Sun, P.; Zhang, H.; Sun, Y.; Liu, J. The Recent Development of Fluorescent Probes for  
447 the Detection of NADH and NADPH in Living Cells and in Vivo. *Spectrochim. Acta. A.*  
448 *Mol. Biomol. Spectrosc.* **2021**, *245*, 118919. <https://doi.org/10.1016/j.saa.2020.118919>.

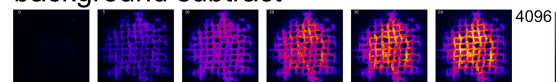
- 449 (34) Park, S. Y.; Yoon, S. A.; Cha, Y.; Lee, M. H. Recent Advances in Fluorescent Probes for  
450 Cellular Antioxidants: Detection of NADH, hNQO1, H<sub>2</sub>S, and Other Redox  
451 Biomolecules. *Coord. Chem. Rev.* **2021**, *428*, 213613.  
452 <https://doi.org/10.1016/j.ccr.2020.213613>.
- 453 (35) Candeias, L. P.; MacFarlane, D. P. S.; McWhinnie, S. L. W.; Maidwell, N. L.; Roeschlaub,  
454 C. A.; Sammes, P. G.; Whittlesey, R. The Catalysed NADH Reduction of Resazurin to  
455 Resorufin. *J. Chem. Soc. Perkin Trans. 2* **1998**, No. 11, 2333–2334.  
456 <https://doi.org/10.1039/a806431h>.
- 457 (36) Hall, M. D.; Simeonov, A.; Davis, M. I. Avoiding Fluorescence Assay Interference—The  
458 Case for Diaphorase. *ASSAY Drug Dev. Technol.* **2016**, *14* (3), 175–179.  
459 <https://doi.org/10.1089/adt.2016.707>.
- 460 (37) Navas Díaz, A.; González García, J. A.; Lovillo, J. Enhancer Effect of Fluorescein on the  
461 Luminol-H<sub>2</sub>O<sub>2</sub>-Horseradish Peroxidase Chemiluminescence: Energy Transfer Process. *J.*  
462 *Biolumin. Chemilumin.* **1997**, *12* (4), 199–205. [https://doi.org/10.1002/\(SICI\)1099-  
463 1271\(199707/08\)12:4<199::AID-BIO445>3.0.CO;2-U](https://doi.org/10.1002/(SICI)1099-1271(199707/08)12:4<199::AID-BIO445>3.0.CO;2-U).
- 464 (38) Zhou, Y.; Du, J.; Wang, Z. Fluorescein and Its Derivatives: New Coreactants for Luminol  
465 Chemiluminescence Reaction and Its Application for Sensitive Detection of Cobalt Ion.  
466 *Talanta* **2019**, *191*, 422–427. <https://doi.org/10.1016/j.talanta.2018.09.007>.
- 467 (39) Rueden, C. T.; Schindelin, J.; Hiner, M. C.; DeZonia, B. E.; Walter, A. E.; Arena, E. T.;  
468 Eliceiri, K. W. ImageJ2: ImageJ for the next Generation of Scientific Image Data. *BMC*  
469 *Bioinformatics* **2017**, *18* (1), 529. <https://doi.org/10.1186/s12859-017-1934-z>.
- 470 (40) Gorbunova, I. A.; Danilova, M. K.; Sasin, M. E.; Belik, V. P.; Golyshchev, D. P.;  
471 Vasyutinskii, O. S. Determination of Fluorescence Quantum Yields and Decay Times of  
472 NADH and FAD in Water–Alcohol Mixtures: The Analysis of Radiative and  
473 Nonradiative Relaxation Pathways. *J. Photochem. Photobiol. Chem.* **2023**, *436*, 114388.  
474 <https://doi.org/10.1016/j.jphotochem.2022.114388>.
- 475 (41) Bueno, C.; Villegas, M. L.; Bertolotti, S. G.; Previtali, C. M.; Neumann, M. G.; Encinas,  
476 M. V. The Excited-State Interaction of Resazurin and Resorufin with Amines in Aqueous  
477 Solutions. Photophysics and Photochemical Reaction. *Photochem. Photobiol.* **2002**, *76*  
478 (4), 385–390. [https://doi.org/10.1562/0031-8655\(2002\)0760385TESIOR2.0.CO2](https://doi.org/10.1562/0031-8655(2002)0760385TESIOR2.0.CO2).  
479

480 **TOC only**



481

background subtract



differential

